Robotics and Computer-Integrated Manufacturing 44 (2017) 208–217

Contents lists available at ScienceDirect

Robotics and Computer-Integrated Manufacturing

journal homepage: www.elsevier.com/locate/rcim

Development of a high speed and precision wire clamp with both position and force regulations

Cunman Liang, Fujun Wang *, Yanling Tian, Xingyu Zhao, Dawei Zhang

Key Laboratory of Mechanism Theory and Equipment Design of Ministry of Education, School of Mechanical Engineering, Tianjin University, Tianjin 300072, China

ARTICLE INFO

Article history:
Received 12 November 2015
Received in revised form
9 July 2016
Accepted 14 September 2016

Keywords:
Wire clamp
Flexure mechanism
Mechanical design
Position/force regulation

ABSTRACT

This paper presents the mechanism and robust control of a monolithic wire clamp to achieve fast and precision operations for strong and robust micro device packaging. The wire clamp is piezoelectrically actuated and a two-stage flexure-based amplification was designed to obtain large and parallel jaw displacements. The grasping forces of the wire clamp were evaluated based on finite element analysis (FEA), and the force measurement was presented. The wire clamp was manufactured using wire EDM technique and the position and force transfer functions were obtained based on the frequency response approach. The position/force switching control strategy was employed to regulate the motion position and grasping force, and the position/force switching controller composed of a PID controller for position control and a sliding model controller (SMC) for force control was designed. Experimental tests were carried out to investigate the performance of wire clamp with the position/force switching controller during the grasping and releasing operations. The results show that the wire clamp exhibits good performance and demonstrate that high speed and precision grasping operations can be realized through the developed wire clamp and the control strategy.

1. Introduction

Recently with the rapid development of microelectronic industries, the demand for electronic products with high pin-count IC installations and high assembly density has been increasingly growing [1–3]. As an important cost-effective and flexible interconnecting technology for micro device packaging, thermosonic wire bonding has been widely used for the microelectronic packaging of nearly any type of daily used electronic products [4]. Automatic wire bonders are important equipments for wire bonding, and high performance wire bonders are required to produce smaller pad size and finer pitch of microelectronic products in extreme conditions [5,6].

As an important component of automatic wire bonders, wire clamps perform high-frequency open and close operations during wire bonding process, and thus the characteristics of wire clamps can directly affect the packaging quality and efficiency [7]. During the extreme motion with short strokes and high acceleration [8,9], there will be some undesired disturbances to the wire and wire clamps, affecting the motion of the clamps, which will further have influence on the bonding quality. As a result, it is necessary to develop high performance wire clamps with a novel mechanism and robust controller to provide stable and high speed microelectronic wire bonding.

In the literature, there are some research reported on the wire clamps, most of which mainly focused on the wire clamp actuators and mechanisms, and little attention has been paid to their position/force control issues. The presently used wire clamps usually adopt electromagnetic and piezoelectric actuators as drivers, and they can realize position tracking using position feedback control. However, few of them have a real-time grasping force controller [10,11]. Even if the grasping forces of some clamps were regulated, the grasping force control was mainly carried out in indirect ways, such as through the installation of preload springs or force calibration, making it difficult to achieve real time and precision force control. However, the robust position/force control is of great importance for the wire clamps to achieve robust and precision grasping and releasing operations.

The position/force control has been receiving considerable attention from the researchers. Impedance control strategy can be used to indirectly regulate the force using a single controller through establishing the dynamic relation between the force and position or velocity. However, the environmental conditions of wire clamps for thermosonic wire bonding are not always certain, which makes it difficult to accurately control the force using the indirectly control approach [12,13]. Through hybrid position/force

* Corresponding author.
E-mail address: wangfujun@tju.edu.cn (F. Wang).

http://dx.doi.org/10.1016/j.rcim.2016.09.006
0736-5845/

control scheme, the grasping and releasing operations can be implemented by controlling the position of the clamp jaws and monitoring the contact forces at the same time, but the control performance largely depends on the division of force and position subspaces, which requires to accurately identify the environmental constrains [14]. To overcome this issue, intelligent control methodologies, such as fuzzy and neural network control, have been proposed to control forces [15,16]. However, the calculation amount becomes larger and the practical implementation process becomes more complicated. Hence, a simple yet efficient approach is desirable to realize the stable and precision force/position control of wire clamps.

Intuitively, a position/force switching control can be used to regulate the grasping jaw position and contact force alternately [17,18]. As for the control scheme, proportional-integral-derivative (PID) controllers have been widely used in industrial applications. However, traditional PID control can not accomplish the wire clamp position/force regulation, because there may be high-frequency dynamic force vibrations when the jaw contacts with the object during the fast grasping and releasing operations. Some advanced control theories including the robust control [19], adaptive control [20], iterative learning control [21] and neural networks control [22], were presented to control precision positioning systems, which show appropriate level of performance. However, their applications are limited in the fast and precision wire clamp control because of the computationally expensive calculations [23]. Sliding mode control has the advantages of fast response and strong robustness for the disturbances, and thus exhibits great potential for the control of high-speed precision wire clamps [24].

This paper presents the mechanism and robust position/force switching control of a novel monolithic piezoelectric actuated wire clamp. Firstly, the mechanism of the wire clamp is introduced. The grasping force is investigated based on finite element analysis (FEA), and the grasping force measurement is presented. The dynamic models of position and force are obtained through frequency response approach, based on which the position/force switching controller, composed of a PID position controller and a sliding model force controller, is designed. The wire clamp is fabricated, and experimental tests are carried out to investigate the performance of the wire clamp and controller.

2. Mechanism and grasping force investigation

2.1. Configuration of the wire clamp

Fig. 1 shows the mechanical structure of the piezoelectric actuated flexure-based wire clamp consisting of a stack piezoelectric ceramic actuator (SPCA), a pair of grasping jaws, a pair of flexible beams, a preload bolt, a base and a flexible motion transmission mechanism designed as a two-stage amplification including a homothetic bridge type mechanism and a parallelogram leverage mechanism. The SPCA is connected with the flexible motion transmission mechanism by the preload bolt at one end of the SPCA, and the preload force to the SPCA can be adjusted by the bolt. Both of the grasping jaws connected with the motion transmission mechanism through two flexible beams, and because of the space limit, a stain gauge is adopted and surface bonded on the left flexible beam to measure the grasping force during the grasping and releasing operations. In order to avoid shear force and bending torque acting on the actuator, the wire clamp is designed symmetrically along the longitudinal axis of the SPCA. Due to the symmetric architecture, the measurement of a single flexible beam is sufficient. A stain gauge is glued on the base end of the flexible beam where is the maximum stress point under the

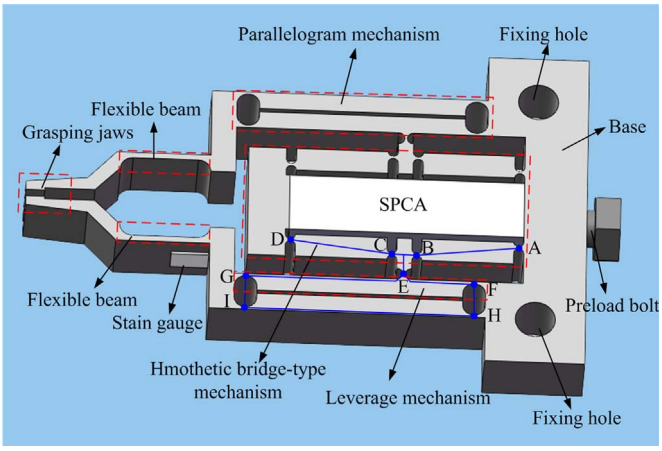

Fig. 1. The mechanism of the wire clamp.

grasping force to generate a high sensitivity and high signal/noise ratio.

Through the two-stage amplification, the motion transmission and displacement amplification from the SPCA to the grasping jaws are realized. As the first-stage amplification the homothetic bridge-type mechanism is composed of a connecting rod mechanism (A-B-C-D) based on double-notch circular flexure hinges, and its working principle is that once actuated with an input displacement, the device produces two vertical output displacements towards the SPCA. In order to obtain a large displacement amplification ratio, a leverage mechanism (E-F-G) integrated within a parallelogram mechanism (F-G-H-I) at each side of the wire clamp is designed as the second-stage amplification connected with the homothetic bridge-type mechanism by two flexure hinges. Through the parallelogram mechanism pure jaw translations can be realized, thus avoiding the sliding between the wire and jaws during the operations, and more stable and firm wire grasping can be ensured due to the fact that the grasping force will act normal to the wire compared with the angular grasping mode.

In order to grasp a wire, a voltage should be applied to the SPCA to make it expand and push the homothetic bridge-type mechanism (A-B-C-D); then the homothetic bridge-type mechanism will pull the leverage mechanisms (E-F-G-H-I), which causes the grasping jaws to close to grasp the manipulated wire. After power is switched off, the SPCA retracts to its initial position, causing the grasping jaws to open and release the manipulated wire.

2.2. Kinematic analysis of the wire clamp

There are various approaches to model a compliant mechanism, such as the pseudo rigid body (PRB) method [25], the compliance matrix method [26], the finite element (FE) method [27] etc. PRB method is utilized to analyze the kinematic characteristics of the wire clamp. Due to the symmetric architecture, only half of the wire clamp is considered and the kinematic model is established as shown in Fig. 2, where i (i=A, B… J) denotes the rotational centers of flexure hinges. From Fig. 2 it is can be seen that A-B-C-D-E-F is equivalent to a six-bar linkage mechanism with one degree of freedom. Based on the geometric and motion relationships the following equations can be get:

$$l_{AB}e^{i\varphi_1} + l_{BC}e^{i\varphi_2} + l_{CD}e^{i\varphi_3} = se^{i\pi/2} \tag{1}$$

$$l_{AB}e^{i\varphi_1} + l_{BE}e^{i(\varphi_2+\alpha)} = l_{AF}e^{i\beta} + l_{EF}e^{i\varphi_4} \tag{2}$$

where s is the distance between the flexure hinges A and D, α is

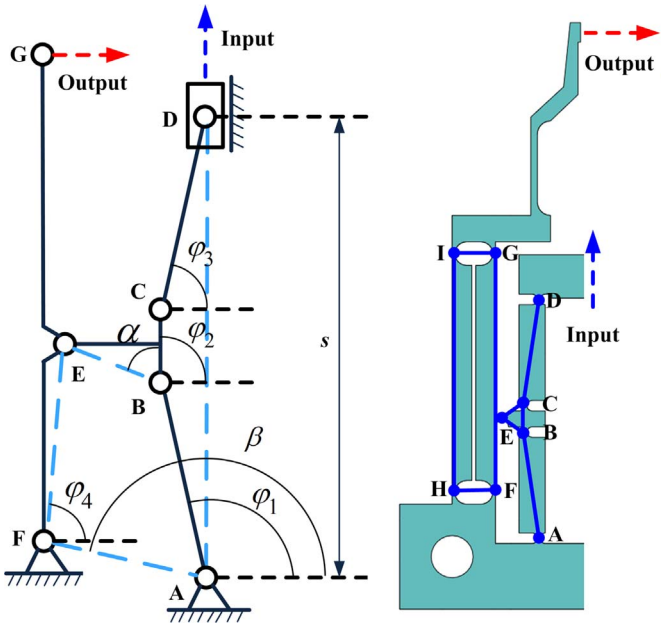

Fig. 2. The kinematic model of the wire clamp.

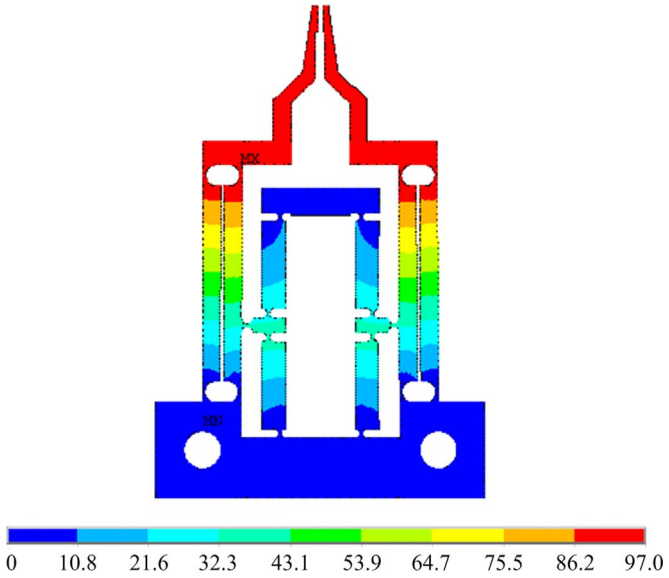

Fig. 3. FEA results of the wire clamp.

the angle between the linkages BC and BE, β is the angle between linkage AF and the x-axis positive direction, l_j (j=AB, BC,…, AF) is the length of the linkage j, φ_1, φ_2, φ_3 and φ_4 are the initial angular positions of the linkages AB, BC, CD and FE, respectively.

Differentiate Eqs. (1) and (2) with respect to time and let the real and imaginary parts be equal. The following equation can be obtained:

$$\mathbf{A}\boldsymbol{\omega} = \mathbf{B}\frac{ds}{dt} \tag{3}$$

where $$\mathbf{A} = \begin{bmatrix} l_{AB}\sin\varphi_1 & l_{BC}\sin\varphi_2 & l_{CD}\sin\varphi_3 & 0 \\ l_{AB}\cos\varphi_1 & l_{BC}\cos\varphi_2 & l_{CD}\cos\varphi_3 & 0 \\ l_{AB}\sin\varphi_1 & l_{BE}\sin(\varphi_2+\alpha) & 0 & -l_{EF}\sin\varphi_4 \\ l_{AB}\cos\varphi_1 & l_{BE}\cos(\varphi_2+\alpha) & 0 & -l_{EF}\cos\varphi_4 \end{bmatrix},$$

$$\boldsymbol{\omega} = \begin{bmatrix} \omega_1 \\ \omega_2 \\ \omega_3 \\ \omega_4 \end{bmatrix}, \quad \mathbf{B} = \begin{bmatrix} 0 \\ 1 \\ 0 \\ 0 \end{bmatrix}.$$

The displacement amplification ratio can be calculated as

$$\lambda = \frac{2d_{out}}{d_{in}} \cong \frac{2\partial d_{out}}{\partial d_{in}} = \frac{2\omega_4 l_{FG}}{\frac{ds}{dt}} = \mathbf{A}^{-1}\mathbf{B}(4,1)l_{FG} \tag{4}$$

where d_{in} and d_{out} are the displacements of input end and moveable jaw, respectively.

From Eq. (4), it can be found that the amplification ratio of the wire clamp has no relations with flexure hinges. The amplification ratio can be calculated of 21.7 depending on the geometric parameters of the linkages.

The kinematic characteristics of the wire clamp were investigated using FEA, and the finite element model was established with the aid of ANSYS software. The actuation displacement was applied by the SPCA on the input terminal of the wire clamp, and the deformation behavior of the jaw as well as flexure hinges and moving linkages under the input displacement of 10 μm applied by the SPCA is shown in Fig. 3. The maximum displacement of a jaw can reach 97 μm which can enable firm and robust grasping operations with a large range of wires. Thus the displacement amplification ratio of the wire clamp is 19.4, which is in good agreement with the calculated result.

2.3. Grasping force analysis

FEA was carried out to analyze the grasping force of the wire clamp. Since the grasping force that the jaws apply on the wire can be affected by the initial position between the jaws and the wire, the sketch of jaws and wire is defined and shown in Fig. 4, where D is the initial distance between the jaws, d is the diameter of wire and δ is the distance between the jaw and wire. The FEA model was established using ANSYS software, and the physical and mechanical parameters of the wire clamp are listed in Table 1.

For FEA, the surfaces of the two fixing holes were fixed through applying zero displacements, and the input displacements with a range from 0 μm to10 μm were applied on the input terminal of the wire clamp and the grasping force under the input displacement was extracted when δ=40 μm, δ=50 μm and δ=60 μm, respectively. The relationship between the grasping force and the input displacement is summarized in Fig. 5. From Fig. 5, it can be

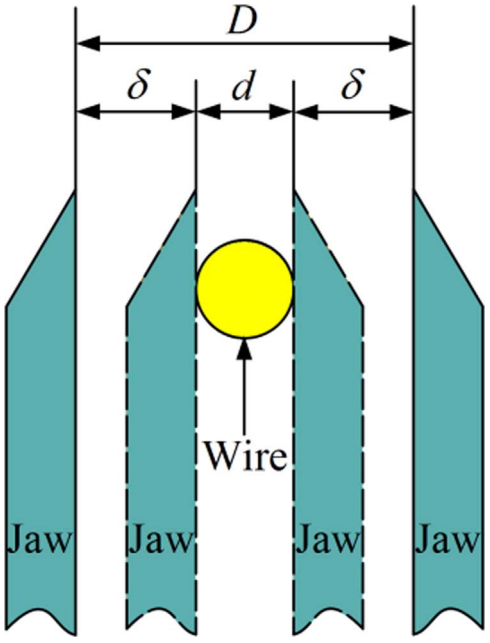

Fig. 4. Sketch of the jaws and wire.

Table 1
Physical and mechanical parameters of the wire clamp.

Parameter	Young's modulus (GPa)	Tensile (MPa)	Poisson' ratio	Density (kg/m^3)
Value	71.7	503	0.33	2810

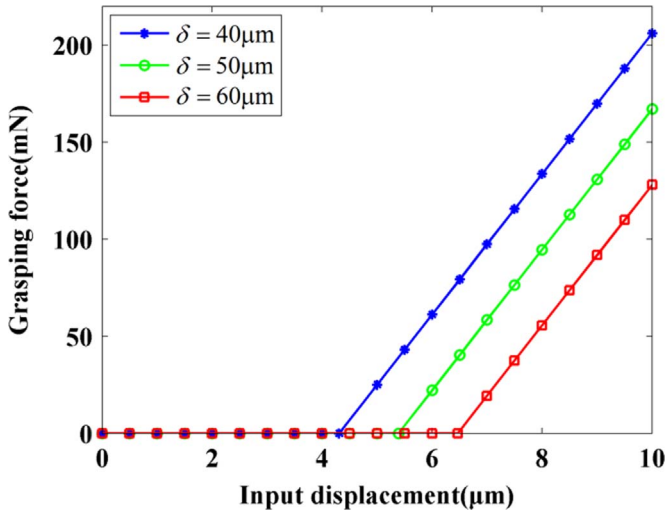

Fig. 5. Relationship between the grasping force and input displacement.

seen that the grasping force is zero before the jaws contact the wire, and increases linearly with the input displacement after contact. When δ=40 μm, δ=50 μm and δ=60 μm, the maximum grasping forces can reach 206.12 mN, 167.08 mN and 128.06 mN, respectively.

2.4. Grasping force measurement

It is necessary to accurately measure the grasping forces before control them. The stain gauge glued on flexible beam can sense the force applied to it as a change in resistance, which is produced by the strain induced by the applied force. In order to reduce the stress concentration of the flexible beam, two fillets are adopted to connect the jaw and end of the parallelogram mechanism, respectively, which is shown in Fig. 1. According to the bending deformation theory of flexible beams, the strain of the flexible beam at the position of the stain gauge can be calculated as

$$\varepsilon_b = \frac{6FL_s}{EBh^2} \tag{5}$$

where F is the grasping force applied on the jaw, L_s is the distance between the point of applying force and the strain gauge, E is the Young's Modulus of the material, B is the beam thickness, and h is the beam width.

The resistance change of the strain gauge is given by

$$\Delta R = \varepsilon_b S_g R_0 \tag{6}$$

where ε_b is the beam strain, S_g is the gauge factor of the strain gauge and R_0 is the nominal resistance of the strain gauge.

The strain gauge is then connected to a Wheatstone bridge whose output is connected to a dynamic strain gauge to amplify the signal. The output voltage of the strain gauge is given by

$$U_{\text{out}} = \frac{n}{4} k_s \varepsilon_b S_g U_b \tag{7}$$

where n denotes the number of the stain gauges in Wheatstone bridge, k_s is the amplification ratio of the dynamic strain gauge, and U_b is the excitation voltage of the Wheatstone bridge.

Substituting Eq. (5) into Eq. (7), yields

$$U_{\text{out}} = \frac{3nk_s L_s S_g U_b}{2EBh^2} F \tag{8}$$

Based on Eq. (8), the following equation can be obtained:

$$F = \Re U_{\text{out}} \tag{9}$$

where $\Re = \frac{2EBh^2}{3nk_s L_s S_g U_b}$.

Eq. (9) describes the relationship between the grasping force applied on the jaw and the output voltage of the strain gauge. It can be found that it is a linear relationship between the grasping force and the output voltage on the condition that the parameters of the flexible beam and the measurement system are certain. Therefore, the grasping force measurement method is feasible.

3. Prototype development and system identification

3.1. Prototype development and experimental setup

Fig. 6 shows the prototype of the wire clamp actuated by a SPCA (type: XP 5 × 5/18, output displacement: 0–18 μm, applied voltage: 0–150 V, maximum driving force: 1400 N). The wire clamp was fabricated through wire electro-discharge machining (wire EDM) technique to guarantee the geometrical accuracy of the crucial sections, and it was made from the material of AL7075-T651, which has the property of high elasticity, yield strength and light mass. The overall dimension of the wire clamp is 45 mm × 28 mm × 5 mm, and the initial gap between the grasping jaws is 500 μm.

A laser displacement sensor (LK-H050 from Keyence, Inc) was employed to measure the position of the grasping jaw, which provides a 50 nm resolution within a 20 mm measuring range. A strain gauge (BE120-1AA from Sichuanger, Inc) was glued on the base end of the flexible beam to form a quarter bridge for the grasping force measurement. The strain gauge has a nominal length and width of 4.3 mm and 3.5 mm, respectively and the gauge factor is 2.22. A dynamic strain gauge (SDY2105) was adopted to measure the dynamic strain of the beam with the aid of the strain gauge and Wheatstone bridge. A voltage amplifier (E505.00 from PI, Inc) was used to amplify the input voltage by an adjustable gain of 10 for the SPCA actuation. The controller system of the prototype was realized by the dSPACE DS1103 controller, which picks up the outputs from the grasping force sensor system and the tip displacement sensor system to determine the state of

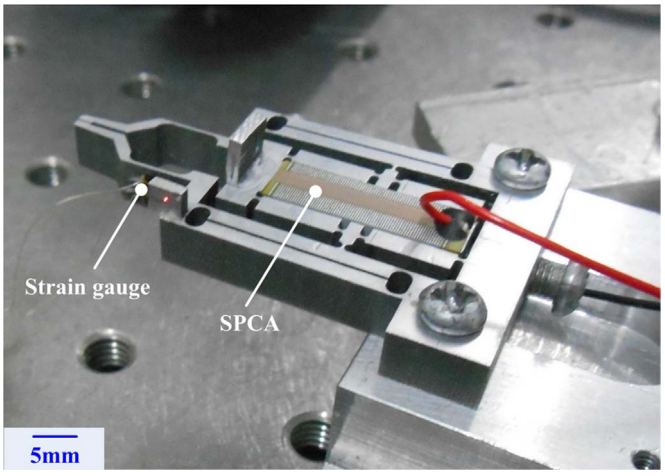

Fig. 6. The prototype of the wire clamp.

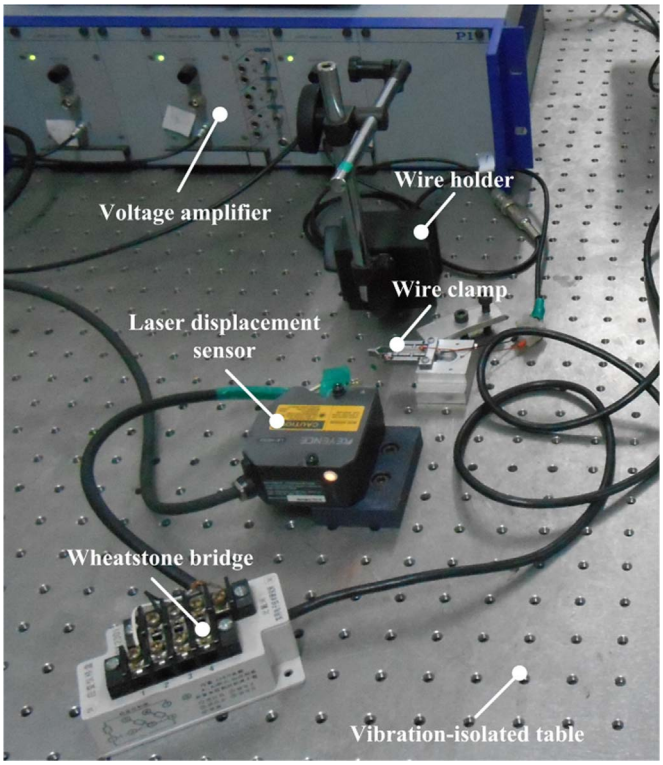

Fig. 7. Experimental setup.

the wire clamp. According to the determined state of the wire clamp, the controller calculates the control algorithm and generates the command voltage, which was applied to the voltage amplifier to realize the corresponding operation. All the devices were placed on a vibration-isolated Newport RS-4000 table and the experimental setup is displayed in Fig. 7.

3.2. System identification

Experimental system identification based on the frequency response was adopted to capture the dynamic model for the design of a controller for the wire clamp. Swept sine waves with the amplitude of 0.6 V and frequency range of 0.1–1200 Hz were produced by a dSPACE DS1103 controller to actuate the SPCA through the voltage amplifier in order to obtain the experimental data to identify the two empirical models for position /force control. During the identification of position model, the wire clamp was operated freely, while a 25.4-μm gold wire was selected as a grasped object to identify force model. The position response was measured by the laser displacement sensor, and the force response was measured by the strain gauge. The output signals of position and force responses were acquired within 10 kHz, and then the Matlab System Identification Toolbox was used to process the data, and the results are summarized in Figs. 8 and 9. The transfer functions of position and force are achieved from the input-output sequences, and they are given as

$$G_s(s) = \frac{-7540s^3 + 4.261\times10^7 s^2 - 3.097\times10^{11}s + 7.422\times10^{14}}{s^4 + 2976s^3 + 3.213\times10^7 s^2 + 7.421\times10^{10}s + 1.496\times10^{14}} \quad (10)$$

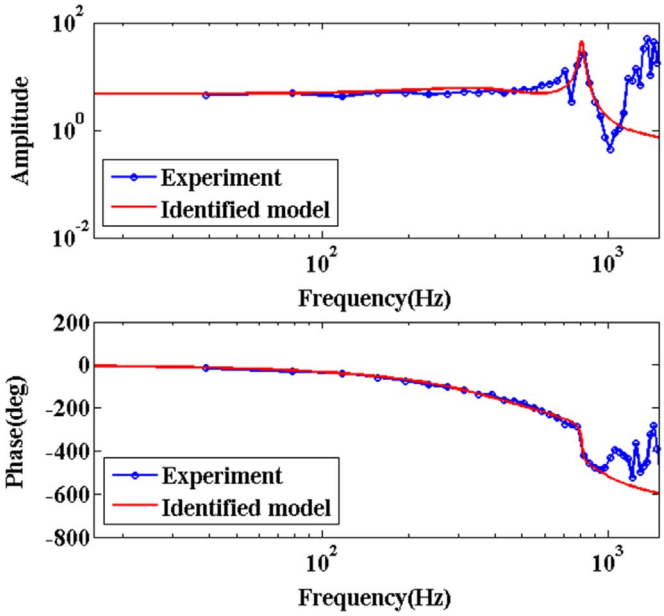

Fig. 8. Results of system identification for the position.

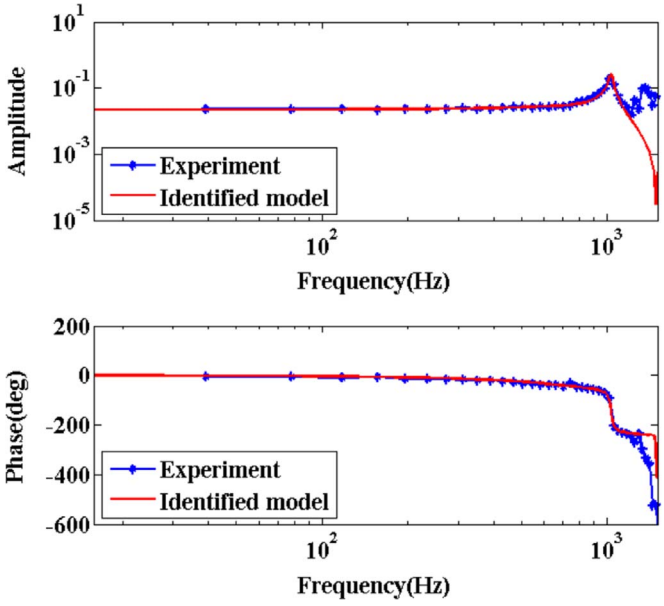

Fig. 9. Results of system identification for the grasping force.

$$G_f(s) = \frac{1.726\times10^6}{s^2 + 217.3s + 4.193\times10^7} \quad (11)$$

4. Position/force switching controller design

4.1. Strategy of position/force switching controller

Since the distance between the two jaws is larger than the diameter of the wire, the grasping task during the working process of wire clamp can be classified into three phases, namely the closing phase, contact phase and opening phase. The closing phase

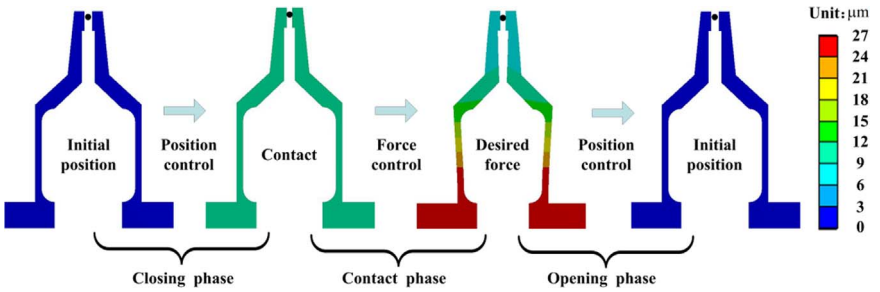

Fig. 10. Strategy of position/force switching control.

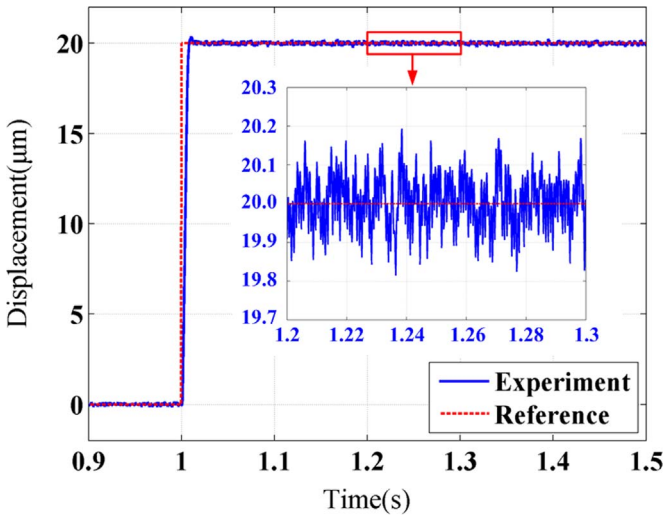

Fig. 11. Displacement step response of the wire clamp.

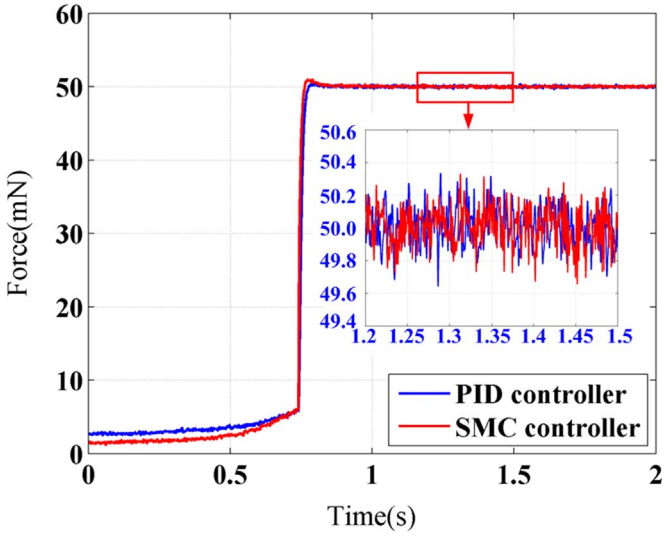

Fig. 12. Results of PID and sliding mode controllers.

occurs prior to the contact of the jaws and wire, the contact phase begins from the touch to the separation of the jaws and wire, and the opening phase is the subsequent time of the jaws motion towards both sides. Precision position control, force control and position control are employed in the closing phase, contact phase and opening phase, correspondingly, which is shown in Fig. 10. In this research, a strategy of position/force switching controller was employed to regulate the position and force alternately. The

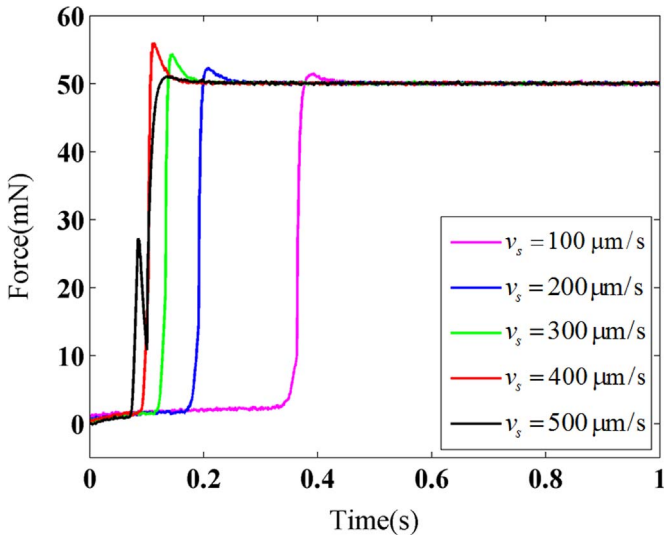

Fig. 13. Results of force control with different switching velocities.

position and force controller design can be seen in Sections 4.2 and 4.3, respectively.

Algorithm 1. position/force switching control (d_r, F_r, F_0, t_0)

```
Initialize (d_r, F_r, F_0, t_0)
if F < f_0 then
    (u_s1) ← position control (d_r): u = f_p(d_r)
else if t < t_0 then
    (u_s2, d_s) ← force control (f_r, u_s1): u = f_F(F_r) + u_s1
else
    position control (d_s, u_s2): u = f_p(d_s) + u_s2
end if
```

Since the same control input voltage applied on the SPCA was adopted in the three phases, the switching between each of the two phases may cause instability or undesired responses of the position and force outputs. In order to guarantee a stable and smooth transition between the two consecutive phases, the final voltage in previous phase should be the base value for the next phase. In this way, a smooth transition between the two phases can be accomplished [28].

The position/force switching control is shown in Algorithm 1, where F_0 is the threshold force, and t_0 is the time to release the wire. During the closing phase, the position control was employed to control the displacement of the grasping jaw following a desired displacement d_r until the grasping force F exceeds the threshold force. The final control voltage u_{s1} can be obtained by the algorithm of position control $f_p(d_r)$. Once the jaws touch the wire and the force sensor indicates the grasping force exceeding the threshold force, the control system switches to the force

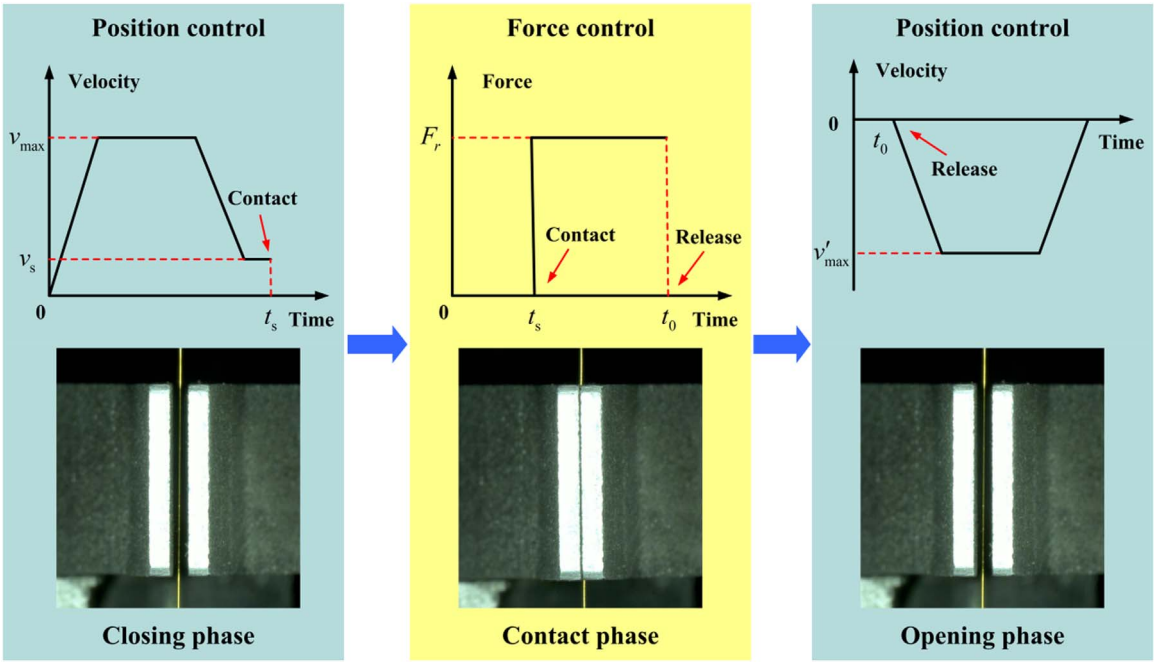

Fig. 14. Trajectory planning of position and force control.

control to regulate the grasping force following the desired force F_r and the control voltage can be obtained through adding the final voltage u_{s1} in the closing phase to the voltage calculated by the algorithm of force control $f_F(F_r)$. When it is time to release the wire ($t > t_0$), the control system will switch to the position control again which controls the jaws to return to the initial position. The control voltage can be calculated based on the final displacement d_s and the final voltage u_{s2} in the contact phase which can be calculated by the algorithm of force control $f_F(F_r)$.

4.2. Position controller

The PID feedback loop has a simple structure, and the parameters of the PID controller are relatively easy to tune. Thus the PID controller was employed to control the displacement of the grasping jaw d to follow a desired displacement trajectory d_r. The transfer function of a traditional PID control can be expressed as

$$G_{PID}(s) = K_P\left(1 + \frac{1}{T_I s} + T_D s\right) \tag{12}$$

where K_P is the proportional gain, T_I is the integral time constant, and T_D is the differential time constant.

Eq. (12) can be written as

$$G_{PID}(s) = K_P + \frac{K_I}{s} + K_D s \tag{13}$$

where $K_I = \frac{K_P}{T_I}$ is the integral gain and $K_D = K_P T_D$ is the differential gain.

Defining $e_d(t) = d_r(t) - d(t)$ as the position error, the PID position controller equation is expressed as following:

$$u_d(t) = K_P e_d(t) + K_I \int_0^t e_d(t)dt + K_D \frac{de_d(t)}{dt} \tag{14}$$

Generally, the PID controller can be adjusted with Ziegler-Nichols (Z-N) method by several simulation studies, and then the parameters are tuned finely through experimental investigations.

4.3. Force controller

Considering there may be some dynamic force vibrations during the contact process, sliding mode control with strong robustness to uncertainties and disturbances has been adopted for the force control. The sliding model controller (SMC) design focuses on the following domains: the selection of the sliding surface and the design of the sliding control law.

Traditional SMC featured with PD-type sliding surface usually produces a slow response speed while the SMC with PID-type sliding surface offers a faster transient response and less steady-state error. Hence, SMC with PID-type sliding surface was designed for the force control. According to the identified transfer function of grasping force, the force model of the wire clamp during the contact phase can be written as

$$\frac{d^2 f(t)}{dt^2} + a_1 \frac{df(t)}{dt} + a_2 f(t) = b_0 u(t) \tag{15}$$

where a_1, a_2 and b_0 are constants, which can be confirmed by Eq. (11).

Assuming there is perturbation of the force system, and the perturbation p can be written as

$$p(t) = \frac{d^2 f(t)}{dt^2} + a_1 \frac{df(t)}{dt} + a_2 f(t) - b_0 u(t) \tag{16}$$

The perturbation can be estimated by

$$p^*(t) = p(t-T) = \frac{d^2 f(t-T)}{dt^2} + a_1 \frac{df(t-T)}{dt} + a_2 f(t-T) - b_0 u(t-T) \tag{17}$$

Then the force model can be expressed as

$$\frac{d^2 f(t)}{dt^2} + a_1 \frac{df(t)}{dt} + a_2 f(t) = b_0 u(t) + p^*(t) + p_e(t) \tag{18}$$

where $p_e(t) = p(t) - p^*(t)$ represents the error between the estimated perturbation and the real perturbation of the system.

In the contact phase, the force controller was designed to control the grasping force f between the grasping jaws and the

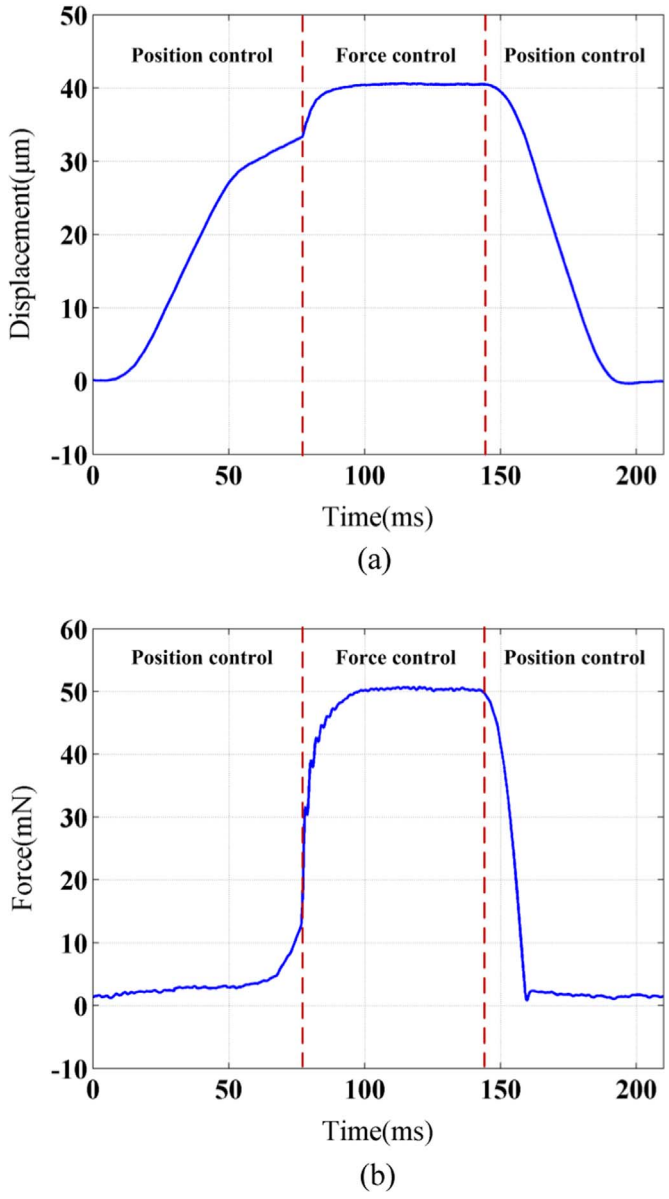

Fig. 15. Results of position/force switching control in the grasp-hold-release operation: (a) displacement response, and (b) force response.

wire to follow a desired force trajectory f_r, and the force error can be defined as

$$e_f(t) = f_r(t) - f(t) \tag{19}$$

Then a sliding function of PID-type can be represented as

$$s(t) = c_P e_f(t) + c_I \int_0^t e_f(\tau)d\tau + \frac{de_f(t)}{dt} \tag{20}$$

where c_P and c_I are positive parameters and the parameters should be chosen strictly Hurwitz.

Designing the sliding control law as

$$u_{SMC} = \frac{1}{b_0}[(a_1 - c_P)\frac{df}{dt} + (a_2 - c_I)f + \frac{d^2f_r}{dt^2} + c_P\frac{df_r}{dt} + c_If_r - p^* - \text{slaw}] \tag{21}$$

The exponential reach law is adopted as the reach law, and it can be expressed as

$$\text{slaw} = -\eta\text{sgn}(s) - ks \tag{22}$$

where $\eta > 0$ and $k > 0$ are constant parameters, and sgn(s) is the sign function.

Define a Lyapunov function as

$$V = \frac{s^2}{2} \tag{23}$$

The first derivate of Eq. (23) can be obtained as

$$\frac{dV}{dt} = s\frac{ds}{dt} \tag{24}$$

Differentiating Eq. (20) with respect to time, yields

$$\frac{ds}{dt} = c_P\left(\frac{df_r}{dt} - \frac{df}{dt}\right) + c_I(f_r - f) + \frac{d^2f_r}{dt^2} + a_1\frac{df}{dt} + a_2f - b_0u - p^* - p_e \tag{25}$$

Then substitute Eqs. (21) and (25) into Eq. (24), and the following equation can be gotten:

$$\begin{aligned}\frac{dV}{dt} &= c_P\left(\frac{df_r}{dt} - \frac{df}{dt}\right)s + c_I(f_r - f)s + \frac{d^2f_r}{dt^2}s + a_1\frac{df}{dt}s \\ &\quad + a_2fs - b_0us - p^*s - p_es \\ &= (-\eta\text{sgn}(s) - ks - p_e)s \\ &= -\eta|s| - ks^2 - p_es\end{aligned} \tag{26}$$

If the gain η is designed to meet the condition

$$\eta > |p_e| + \varepsilon \tag{27}$$

where $\varepsilon > 0$ is an arbitrary constant, then the following relationship can be obtained:

$$\frac{dV}{dt} = -\eta|s| - ks^2 - p_es < -ks^2 - \varepsilon|s| < 0 \tag{28}$$

Eq. (28) implies that the system is stable and the trajectory reaches the sliding surface in finite time and remains on the sliding surface $s=0$. Besides, it also ensures that the states will be confined to the surface $s=0$ for all future time since leaving the surface requires $\frac{dV}{dt}$ to be positive, which is impossible as implied by the inequality.

Due to changes in the function sgn (s), when s is next to zero, the chattering problem can appear. To avoid this undesirable

Table 2
Comparison with other similar works.

Actuation	Amplification ratio	First vibration frequency (Hz)	Overall operation time (s)	Position/force control	Reference
Thermo-Piezoelectric	–	667	120	Yes	[30]
Voice coil motor	–	–	> 1	No	[31]
Piezoelectric	–	500	–	Yes	[32]
PZT	14.8	244	> 5	Yes	[28]
PZT	16	359.56	> 12	No	[33]
PZT	19.4	810	0.2	Yes	This works

effect, the sign function is substituted by a saturation function with the following form:

$$\mathrm{sat}(s) = \begin{cases} 1, & s > \Delta \\ \dfrac{s}{\Delta}, & |s| \le \Delta \\ -1, & s < -\Delta \end{cases} \tag{29}$$

where the positive constant Δ represents the boundary layer thickness, which ensures that s is always bounded by Δ.

The sliding control law can be written as

$$u_{\mathrm{SMC}} = \frac{1}{b_0}[(a_1 - c_{\mathrm{P}})\frac{df}{dt} + (a_2 - c_{\mathrm{I}})f + \frac{d^2 f_r}{dt^2} + c_{\mathrm{P}}\frac{df_r}{dt} + c_{\mathrm{I}} f_r - p^* + \eta\,\mathrm{sat}(s) + ks] \tag{30}$$

5. Experiments

Several control experiments were carried out to examine the performance of the position/force switching controller. During the experiments, gold wires with a diameter of 25.4 μm were employed to verify the effectiveness of the switching control strategy.

5.1. Position control

Step response was investigated and the desired displacement trajectory was defined as a step signal with a final value as 20 μm. The parameters of the position PID controller are chosen as: $K_{\mathrm{P}}=0.016$, $K_{\mathrm{I}}=45$, $K_{\mathrm{D}}=0.002$. The step response of the position control is shown in Fig. 11. From the result it can be seen that the setting time is 12 ms, the overshoot is 2.5%, and the steady-state error is ± 0.2 μm.

5.2. Force control

To compare the performance of PID force controller and sliding mode force controller, step response was investigated and the desired force trajectory was defined as a step signal with a final value as 50 mN. The parameters of the force PID controller are chosen as: $K_{\mathrm{P}}=0.5$, $K_{\mathrm{I}}=2100$, $K_{\mathrm{D}}=0.0015$ and the parameters of the sliding mode controller are chosen as $c_{\mathrm{I}}=720$, $c_{\mathrm{P}}=129600$, $\eta=20$, $k=7500$. These parameters are adjusted by trial and error through experimental studies. Besides the threshold force F_0 is 5 mN. The results of PID and sliding mode controllers are shown in Fig. 12. From the results it can be seen that the setting time of PID controller is 30 ms, the overshoot is 1.3%, and the steady-state error is ± 0.4 mN. The setting time of sliding mode controller is 20 ms, the overshoot is 1.8%, and the steady-state error is ± 0.4 mN. It can be seen that the setting time of sliding mode controller is less than that of PID controller.

5.3. Position/force switching controller

The jaw velocity in the closing phase is important in the transition between the closing phase and contact phase, which can cause instability and undesired responses of the force output. A series of experiments about different velocities have been conducted. The PID controller was employed to control the displacement of the grasping jaw, while the sliding mode controller was utilized to control the grasping force. The parameters of controllers are the same with those in Sections 5.1 and 5.2. In the closing phase the jaw was controlled by PID position controller to close at different velocities of 100 μm/s, 200 μm/s, 300 μm/s, 400 μm/s, and 500 μm/s until the grasping force arrives at the threshold force F0. Then the grasping force was controlled by the sliding mode force controller. The results of force control with different switching velocities are shown in Fig. 13. It can be seen that the overshoots increase with the increase of switching velocities from 100 μm/s to 400 μm/s. The chattering phenomenon which causes instability appears in the force response at velocity of 500 μm/s. Thus the switching velocity can be in 0–500 μm/s to alleviate the chattering effect. The chattering phenomenon may be caused by the jaw inertia or the controller and the related research has been done in different applications [29]. In order to avoid the chattering phenomenon fast control is required, which will be studied in future work.

In order to achieve a complete and efficient grasp-hold-release operation, the position and force trajectories were planned and shown in Fig. 14. During the closing phase the homothetic trapezoidal velocity planning was employed to control the jaw displacement, leading to the contact of the jaws and wire with a constant velocity. In the contact phase a step force signal was utilized as the reference signal of the grasping force. In order to make the jaws return to their initial positions, the trapezoidal velocity planning was used based on the final position in the contact phase.

Fig. 15 shows the results of position/force switching control in the grasp-hold-release operation. The parameters of position and force controller are the same with those in Sections 5.1 and 5.2. A switching velocity of 200 μm/s and switching time ts of 75 ms were chosen in the closing phase, and the desired force trajectory was defined as a step signal with a final value as 50 mN in the contact phase. Besides the threshold force of 10 mN was chosen to realize the switching from the closing phase to contact phase. The results show that the steady-state error of grasping force is ± 0.4 mN, the setting time is 20 ms and the overall time of the operation is within 200 ms. The results are compared with those reported in some similar works which are summarized in Table 2. It is found that the developed wire clamp outperforms the others in terms of a larger amplification ratio, high first vibration frequency and faster overall operation time.

6. Conclusion

In this paper, the mechanism, characteristics and control of a novel piezoelectric actuated wire clamp have been reported. The grasping forces have been investigated based on FEA, and the grasping force measurement has been described. Based on frequency response approach, the transfer functions of position and force were achieved. A position/force switching controller has been designed and employed to regulate the position and force alternately, which is composed of a PID controller for the position control and a slide model controller (SMC) for the force control. Experimental tests have been carried out to investigate the performance of the wire clamp and the position/force switching controller during the grasp-hold-release operation. The position step response shows that the setting time is 12 ms, the overshoot is 2.5%, and the steady-state error is ± 0.2 μm. For the force step response, the results show that the setting time of PID controller is 30 ms, the overshoot is 1.3%, and the steady-state error is ± 0.4 mN. The setting time of SMC is 20 ms, the overshoot is 1.8%, and the steady-state error is ± 0.4 mN. Obviously, the sliding mode force controller outperforms the PID force controller in terms of the setting time. A series of experiments about different velocities have been conducted, the result shows that the chattering phenomenon which may cause instability appears in the force response at velocity of 500 μm/s, and the switching velocity can be in 0–500 μm/s to avoid the chattering effect. The control method to avoid the chattering effect will be studied in future

works. Finally position/force switching control in the grasp-hold-release operation has been investigated based on position and force trajectory planning. The constant force regulation has been realized within 200 ms with the steady-state force error $\pm$ 0.4 mN. The experiment results show that the wire clamp exhibits good performance and demonstrate that the new wire clamp and the control law are well suited for fast and high precision grasping and releasing operations.

Acknowledgments

The supports of this work by the National Natural Science Foundation of China (Grant nos. 51675376 and 51205279), the Science & Technology Commission of Tianjin Municipality (Grant no. 13JCQNJC04100), the Open Project of State Key Laboratory of Special Vehicles and Their Drive System Intelligent Manufacturing, and the Tianjin University for Peiyang Elite Scholar (Grant no. 60301014) are gratefully acknowledged.

References

[1] M.N.M. Zubir, B. Shirinzadeh, Y. Tian, Development of a novel flexure-based microgripper for high precision micro-object manipulation, Sens. Actuators A: Phys. 150 (2) (2009) 257–266.
[2] H. Zhang, F. Wang, X. Zhao, D. Zhang, Y. Tian, Electrical matching of a piezoelectric ultrasonic transducer for microelectronic bonding, Sens. Actuators A: Phys. 199 (1) (2013) 241–249.
[3] Y. Li, Q. Xu, A novel piezoactuated XY stage with parallel, decoupled, and stacked flexure structure for micro-/nanopositioning, IEEE Trans. Ind. Electron. 58 (8) (2011) 3601–3615.
[4] F. Wang, X. Zhao, D. Zhang, Z. Ma, X. Jing, Robust and precision control for a directly driven XY table, Proc. IMechE Part C: J. Mech. Eng. Sci. 255 (5) (2011) 1107–1120.
[5] Z.W. Zhong, Overview of wire bonding using copper wire or insulated wire, Microelectron. Reliab. 51 (1) (2011) 4–12.
[6] F. Wang, J. Li, S. Liu, X. Zhao, D. Zhang, Y. Tian, An improved adaptive genetic algorithm for image segmentation and vision alignment used in microelectronic bonding, IEEE/ASME Trans. Mechatron. 19 (3) (2014) 916–923.
[7] F. Wang, D. Fan, Modeling and experimental study of a wire clamp for wire bonding, J. Electron. Packag. 137 (1) (2015) 011012.
[8] J. Liu, Y. Shi, P. Li, J. Tang, R. Zhao, H. Zhang, Experimental study on the package of high-g accelerometer, Sens. Actuators A: Phys. 173 (1) (2012) 1–8.
[9] F. Wang, X. Zhao, D. Zhang, Y. Wu, Design and control of a directly-driven bond head for thermosonic bonding, Proc. IMechE Part C: J. Mech. Eng. Sci. 224 (4) (2010) 805–815.
[10] D.M. Dozor, Magnetostrictive wire bonding clamp for semiconductor packaging: Initial prototype design, modeling, and experiments, in: Proceedings of SPIE - Industrial and Commercial Applications of Smart Structures Technologies, CA, USA, 1998: 3326: 516–526.
[11] D.K. Fan, F.L. Wang, Finite element analysis of wire clamp for wire bonding, in: Proceedings of International Conference on Electronic Packaging Technology & High Density Packaging, Guilin, China, 2012: 955–958.
[12] A. Pequegnat, H.J. Kim, M. Mayer, Y. Zhou, J. Persic, J.T. Moon, Effect of gas type and flow rate on Cu free air ball formation in thermosonic wire bonding, Microelectron. Reliab. 51 (1) (2011) 43–52.
[13] C.T. Su, C.J. Yeh, Optimization of the Cu wire bonding process for IC assembly using Taguchi methods, Microelectron. Reliab. 51 (1) (2011) 53–59.
[14] M. Rakotondrabe, I.A. Ivan, Development and force/position control of a new hybrid thermo-piezoelectric microgripper dedicated to micromanipulation tasks, IEEE Trans. Autom. Sci. Eng. 8 (4) (2011) 824–834.
[15] C. Treesatayapun, Grasping force controller for parallel grip with fuzzy rules emulated networks, Int. J. Adv. Manuf. Technol. 68 (2013) 45–55.
[16] S. Wen, W. Zheng, J. Zhu, X. Li, S. Chen, Elman fuzzy adaptive control for obstacle avoidance of mobile robots using hybrid force/position incorporation, IEEE Trans. Syst. Man Cybern. Part C: Appl. Rev. 42 (4) (2012) 603–608.
[17] N. Shimada, T. Yoshioka, K. Ohishi, T. Miyazaki, Novel force-sensor-less contact motion control for quick and smooth industrial robot motion, in: Proceedings of the IECON 2011-37th Annual Conference on IEEE Industrial Electronics Society, 2011: 4238–4243.
[18] B. Gao, J. Shao, G. Han, G. Sun, X. Yang, D. Wu, Using fuzzy switching to achieve the smooth switching of force and position, Appl. Mech. Mater. 274 (2012) 638–641.
[19] Q. Xu, New robust position and force regulation for a compliant microgripper, in: Proceedings of the 2013 IEEE International Conference on Automation Science and Engineering, 2013: 801–806.
[20] Q. Xu, M. Jia, Model reference adaptive control with perturbation estimation for a micropositioning system, IEEE Trans. Control Syst. Technol. 22 (1) (2014) 352–359.
[21] B.E. Helfrich, C. Lee, D. Bristow, X.H. Xiao, J. Dong, A.G. Alleyne, S.M. Salapaka, P.M. Ferreira, Combined-feedback control and iterative learning control design with application to nanopositioning systems, IEEE Trans. Control Syst. Technol. 18 (2) (2010) 336–351.
[22] Y. Li, Q. Xu, Design and robust repetitive control of a new parallel-kinematic XY piezostage for micro/nanomanipulation, IEEE/ASME Trans. Mechatron. 17 (6) (2012) 1120–1132.
[23] F. Wang, Z. Ma, W. Gao, X. Zhao, Y. Tian, D. Zhang, C. Liang, Dynamic modeling and control of a novel XY positioning stage for semiconductor packaging, Trans. Inst. Meas. Control 37 (2) (2015) 177–189.
[24] Y. Li, Q. Xu, Adaptive sliding mode control with perturbation estimation and PID sliding surface for motion tracking of a piezo-driven micromanipulator, IEEE Trans. Control Syst. Technol. 18 (4) (2010) 798–810.
[25] C. Liang, F. Wang, Y. Tian, X. Zhao, H. Zhang, L. Cui, D. Zhang, P. Ferreira, A novel monolithic piezoelectric actuated flexure-mechanism based wire clamp for microelectronic device packaging, Rev. Sci. Instrum. 86 (4) (2015) 045106.
[26] N. Lobontiu, In-plane compliances of planar flexure hinges with serially connected straight-and circular-axis segments, J. Mech. Des. 136 (12) (2014) 122301.
[27] G. Palmieri, M.C. Palpacelli, M. Callegari, Study of a fully compliant u-joint designed for minirobotics applications, J. Mech. Des. 134 (11) (2012) 111003.
[28] Q. Xu, Design and smooth position/force switching control of a miniature gripper for automated microhandling, IEEE Trans. Ind. Inform. 10 (2) (2014) 1023–1032.
[29] A. Borboni, F. Aggogeri, A. Merlo, N. Pellegrini, C. Amici, PKM mechatronic clamping adaptive device, Int. J. Adv. Robot. Syst. 12 (2015) 42.
[30] M. Rakotondrabe, I.A. Ivan, Development and force/position control of a new hybrid thermo-piezoelectric microgripper dedicated to micromanipulation tasks, IEEE Trans. Autom. Sci. Eng. 8 (4) (2011) 824–834.
[31] J. Park, S. Kim, D. Kim, B. Kim, S. Kwon, J. Park, K. Lee, A monolithic compliant piezoelectric-driven microgripper: design, modeling, and testing, IEEE/ASME Trans. Mechatron. 10 (5) (2005) 601–606.
[32] Q. Xu, Precision position/force interaction control of a piezoelectric multimorph microgripper for microassembly, IEEE Trans. Autom. Sci. Eng. 10 (3) (2013) 503–514.
[33] D.H. Wang, Q. Yang, H.M. Dong, A monolithic compliant piezoelectric-driven microgripper: design, modeling, and testing, IEEE/ASME Trans. Mechatron. 18 (1) (2013) 138–147.